Probing the Brønsted acidity of the external surface of Faujasite type zeolites

Louwanda Lakiss[†], Aurélie Vicente[†], Jean-Pierre Gilson[†]*, Valentin Valtchev[†], Svetlana Mintova[†], Alexandre Vimont[†], Robert Bedard[‡], Suheil Abdo[‡]*, Jeffery Bricker[‡]

† Normandie Univ, ENSICAEN, UNICAEN, CNRS, Laboratoire Catalyse et Spectrochimie, 14000 Caen, France

‡ UOP LLC, 25 East Algonquin Road, Des Plaines, IL 60016, USA

ORCID Numbers of authors:

Louwanda Lakiss : https://orcid.org/0000-0002-6693-3773

Jean-Pierre Gilson : https://orcid.org/0000-0002-3543-8163

Valentin Valtchev : https://orcid.org/0000-0002-2341-6397

Svetlana Mintova : https://orcid.org/0000-0002-0738-5244

Alexandre Vimont : https://orcid.org/0000-0001-9799-6024

KEYWORDS: Faujasite, Triphenylphosphine oxide, 2,4,6 Tri-tert-butylpyridine, phosphorous NMR spectroscopy, Infrared spectroscopy.

ABSTRACT: We outline two methodologies to selectively characterize the Brønsted acidity of the external surface of FAU-type zeolites by IR and NMR spectroscopy of adsorbed basic probe molecules. The challenge and goal are to develop reliable and quantitative IR and NMR methodologies to investigate the accessibility of acidic sites in the large pore FAU-type zeolite Y and its mesoporous derivatives often referred to as ultrastable Y (USY). The accessibility of their Brønsted acid sites to probe molecules (n-alkylamines, n-alkylpyridines, n-alkylphosphine- and phenylphosphine-oxides) of different molecular sizes is quantitatively monitored either by IR or ^{31}P NMR spectroscopy. It is now possible, for the first time to quantitatively discriminate between the Brønsted acidity located in the microporosity and on the external surface of large pore zeolites.

INTRODUCTION

Zeolite catalysts are currently widely used in oil refining and petrochemical processes and their applications are set to grow further in these classical and other more emerging applications. ([1,2,3,4,5,6]) Their high surface areas and micropore volumes, tunable acidity, active sites located in confined spaces, unique shape selectivity and many other easily adjustable properties make them often the catalysts or adsorbents of choice for various industrial processes. ([2,3,4]) These desired properties come at a price, internal mass transport limitations lowering their potential catalytic performances,([7]) although such limitations can also be effective tools to engineer unique selectivities.([8]) The interplay between internal mass transport and chemical kinetics in zeolite catalysis is often described using the Thiele modulus (Φ) approach.([7]) However, as it explicitly does not take into account the external surface of zeolites, the approach might become less relevant when effective particle size decreases during top-down (biased or unbiased demetallation generating intracrystalline mesoporosity) or bottom-up (direct synthesis of nanosized zeolite crystals generating intercrystalline mesoporosity) hierarchization procedures.([9]) When the external surface of zeolites, where confinement differs from inside the microporosity, is explicitly taken into account in computing the Thiele modulus, it was shown recently that its effect on catalyst effectiveness (η) decreases.([10]) Although impressive advances in the last few years enabled a better description of the micro- and meso-porous volumes and surfaces of zeolites by physisorption of

Nitrogen, Argon and Krypton at low temperatures, these methods do not provide any information on the surface acidity.([11]) In principle, the external surface acidity should increase with added mesoporosity and decreasing crystal size, but zoning can occur due either to synthesis conditions or biased post-synthesis treatments leading to unpredictable acid site concentrations.([12,13,14])

Moreover, zeolite powders are always shaped in the presence of a binder when used in industrial processes. This is required to optimize many, often conflicting, specifications such as mechanical and thermal resilience, pressure drop and hydrodynamics management in the reactor...([15]) During such an operation, a zeolite powder is successively mixed and kneaded with an inorganic binder precursor (e.g. pseudoboehmite) and other additives (peptizing agents, porogens, filler…), shaped (yielding so called green extrudates), dried and then calcined at temperatures above 800 K. Under such conditions, chemical interactions between inorganic binders and zeolite surfaces are likely to occur. As reported elsewhere, zeolite surface properties and more specifically their external acidity are affected during these operations altering their catalytic performances.([16]) Zeolite acidity is multifarious (*e.g.* nature, number, strength, location and distribution across the crystallites, confinement, accessibility…). The potential differences in accessibility and confinement between acid sites located anywhere in the microporosity (hereinafter referred to as internal acidity) and on the external surface of crystallites or any mesoporosity (hereinafter referred to as external acidity) are particularly important.([17,18,19])

Numerous techniques are currently used to characterize the acidic properties of zeolites such as ammonia and alkylamines ([20]) temperature-programmed desorption (TPD), ([21,22]) infrared spectroscopy (IR), ([23,24,25,26,27,28,29,30,31]) and nuclear magnetic resonance (^{1}H and ^{31}P NMR) spectroscopy of adsorbed basic probe molecules. ([32,33])

The number of acid sites determined by adsorption of probe molecules is often lower than expected from their framework (Si/Al) composition, ([34]) due to their accessibility to probe molecules. This led to the definition of an accessibility index (ACI), the ratio between the maximum number of acid sites determined by a given probe molecule and the number expected from their framework composition.([35]) An alternative approach to estimate the acid site density is the consecutive adsorption of probe molecules of decreasing size to better discriminate acid sites distributed in various environments.([36,37]) For instance, the accessibility of the acid sites of mordenite (located either in large channels or more confined side-pockets) and mesoporous derivatives was determined by the consecutive adsorption of substituted alkylpyridines (2,4,6-triethylpyridine 2,4,6-trimethylpyridine and pyridine) and carbon monoxide. ([37]) Recently, Freitas et al. also used IR spectroscopy of alkylpyridines to map the accessibility of acid sites in MFI and BEA zeolites. They highlight that 2,6-dimethylpyridine accesses 50 % of the acidic sites in ZSM-5 while 2,4,6 trimethylpyridine and 2,6 di-tertbutylpyridine reach only 8 and 5 % of the acidic sites, respectively.([38]) Nitriles probes with different sizes were also used to differentiate external and internal acid sites present in ZSM-5 zeolites.([39]) Other probe molecules were also used to determine acid sites accessibility in zeolite such as FER, BEA, ZSM-5 and MCM-([22.31,40,41,42,43]) Another, yet unexplored, option could be the deuteration of acid sites by molecules of increasing sizes, initially developed to map the accessibility of silanols in amorphous silicas.([44]) ^{31}P NMR spectroscopy, with its large window of chemical shifts and easy quantification (natural abundance and spin ½) is becoming popular to measure zeolite acidity with phosporous probes: trimethylphosphine oxide is a good example as it provides information on the number, type (Lewis and Brønsted) and strength of zeolitic acid sites.([33,38,45,46,47,48,49,50,51]) Earlier analyses, performed with trimethylphosphine (TMP) ([52,53]) are now replaced by the more stable and less hazardous alkylphosphine oxides. Trimethylphosphine oxide (TMPO), for instance, was used to probe acidity in amorphous silica–aluminas, aluminas, and zeolites.([46]) Mafra et al. used a combination of alkylphosphine oxides of different sizes (trimethylphosphine [TMPO, kinetic diameter: 0.55 nm]) and tributylphosphine oxide [TBPO, kinetic diameter: 0.82 nm]), to successfully discriminate the internal from the external acidity of ZSM-5 zeolites.([50]) Chemical reactions should be the ultimate way to assess the acidity and catalytic activity of the external surface of zeolites ([54,55,56]) but it is often challenging to prove that either reactants, intermediates or some products do not penetrate their microporosity at reaction temperatures.

As far as industrial applications are concerned, it is well recognized that Brønsted acid sites located on the external surface (*e.g.* MWW) or at the pore-mouths (*e.g.* MTT, TON…) of some zeolites, are the active sites for some important reactions as cumene synthesis and the selective hydroconversion of long-chain n-paraffins to their mono-branched isomers.([57]) On the other hand, when p-xylene is produced industrially on MFI-based catalysts, either by mixed xylene isomerization, toluene disproportionation or alkylation, their external surface active sites are selectively deactivated by reaction with, for instance, organo-nitrogen or -phosphorous compounds.([58,59])

So far, all methodologies describing the acidity of the external surface of zeolites fail when applied to the FAU structure, in its purely microporous form (Y) and even more on its mesoporous derivatives (USY). A ^{31}P NMR study of rare earth zeolite Y using TMPO and TBPO reported that TBPO does not access zeolite Y microporosity and estimated its concentration of external acidic sites at 120 µmol/g, i.e. about 3 % of the total acid sites.([45]) However, this zeolite, with a Si/Al ratio of 3.7, was certainly dealuminated, *i.e.* already possessed some mesoporosity as well as extraframework species potentially restricting the accessibility of some probe molecules; this could raise doubts on the accessibility of TBPO to the native microporosity of zeolite Y.

The FAU type structure is by far the most widely used zeolite in industrial processes: *i*) the so-called Y or USY (Si/Al ≥ 2.5) mostly as a catalyst (Hydrocracking, Fluid Catalytic Cracking [FCC], Aromatics alkylation...) ([6]), *ii*) the so-called X (Si/Al ~ 1.0) mostly as an adsorbent (aromatics separations…). Its crystalline structure, made of sodalite

cages (cuboctahedral units) linked by hexagonal prisms (double six rings), generates a microporosity in supercages of about 1.2 nm in diameter accessible to relatively bulky molecules; ([60]) the sodalite cages remain inaccessible to most probe molecules unless opened by chemical treatment. ([61]) As-synthesized Y zeolite is usually in its sodium form and acidity generated by ammonium exchange(s) followed by calcination(s). During calcination, partial dealumination and/or amorphisation can occur. Zeolite Y is often dealuminated by steaming at high temperatures and/or acid leaching to prepare a more stable form, the so-called ultrastable Y (USY). During this process, some aluminum is expelled from the framework and mesoporosity added to its native microporosity creating a hierarchical material, provided micro- and meso-porosity are sufficiently connected. The acidic (number, strength, location, accessibility, distribution…) and textural properties of the zeolite are therefore modified during this process. In particular, the confinement in a significant proportion of acid sites will change as the microporosity will decrease and intracrystalline mesoporosity will be added, i.e. the internal/external acidity ratio will increase. This ratio is also substantially increased, with the formation of intercrystalline mesoporosity, when small crystals (< 100 nm) of zeolites are synthesized, the so-called nanozeolites.([62,63])

In IR spectroscopy, the preferred methodology to quantify acid properties, the stepwise addition of calibrated doses of a basic probe molecule is the norm. It is however a challenge to find suitable probe molecules (liquid with a vapor pressure of about 0.1 torr) not entering the zeolite Y microporosity due to the dimension (0.74 nm) of the windows (12 MR, twelve T atoms delineating a ring) leading to its supercages. Two criteria need consideration when selecting such suitable probe molecules: their kinetic diameter and the adsorption temperature. A trusted rule of thumb states that molecules with a kinetic diameter 20 % larger than a zeolite pore will enter the porosity as temperature increases.([55,64]) Accordingly, a molecule probing the external surface of FAU type structures should have a kinetic diameter superior to 0.9 nm. ([55]) 2,4 dimethylquinoline (2,4 DMQ) is a potential candidate and was already used to probe the external acidity of some zeolites.([31]) As it accesses, at 423 K, the microporosity of BEA and FAU structures, lowering its adsorption to room temperature might prevent or significantly delay its diffusion in the FAU microporosity.

We screened other basic molecules using these criteria to monitor the FAU external surface acidity by IR (2,4 dimethylquinoline [DMQ, 0.91 nm], 2,6 di-tert-butylpyridine [DTBPy, 0.8 nm], 2,4,6 tri-tert-butylpyridine [TTBPy, 1.1 nm]) or ^{31}P NMR (triphenylphosphine oxide [TPhPO, 1.1 nm]) spectroscopies. In addition, as trimethylamine (TMA) was already used to measure the strength of acid sites in zeolite Y, we selected two bulkier alkylamines (tributylamine [TBA, 1.1 nm] and trihexylamine [THA, 1.3 nm]). 30 The more classical probes, Pyridine (IR) and TMPO (NMR) were used to quantify the maximum accessible acidity of zeolite Y and its USY derivatives. These probe molecules along with some selected properties are described in Table S.1.

EXPRIMENTAL SECTION

Three commercial zeolites were investigated: *i*) Y: LZY-64 supplied by UOP, *ii*) USY's: CBV720 and CBV760 purchased from Zeolyst. Some typical physicochemical properties are summarized in Table 1. USY's are typical of steamed (CBV720) and steamed/acid leached (CBV760) Y zeolites. Their Si/Al ratios range from 2.3 to 28 and they differ significantly by their acidic and textural properties. As expected, USY's display higher mesoporosity than their Y parent.

Probe molecules with different sizes and basicities, namely Pyridine (Py, 99.8 %), 2,6 Di-tert-butylpyridine (DTBPy, >97 %), 2,4 Dimethyl quinoline (DMQ, 95%), Tributylamine (TBA, 99.5 %), Trihexylamine (THA, 96 %) and 2,4,6 Tri-tert-butylpyridine (TTBPy, 99%) were purchased from Sigma-Aldrich and used without further purification.

With the exception of Py, DTBPy and TTBPy, the molar absorption coefficients of bands characteristic of the protonated probe molecules were not determined. Instead, the Brønsted acid site concentrations were measured by integrating the ν(OH) bands at 3630 cm^{-1} (OH_{HF}, located in the supercages) and 3550 cm^{-1} (OH_{LF}, located in the sodalite cages) before and after adsorption of the probe molecules. Their respective molar absorption coefficients (ε OH_{HF} = 6.76 cm.mol^{-1} and ε OH_{LF} = 5.39 cm.mol^{-1}) were determined, very accurately, earlier in a homemade setup (AGIR), by monitoring simultaneously weight gains/losses on a thermobalance (AG) fitted with a cell recording the IR spectra of the adsorbed probes.([24])

IR spectra were recorded with a Nicolet Magna 550-FT-IR spectrometer at 4 cm^{-1} optical resolution. Prior to the measurements, the zeolites were pressed into self-supporting discs (diameter: 1.6 cm, 18 mg) and pretreated in the IR cell attached to a vacuum line (10^{-6} Torr), first at 393 K for 2 hours followed by a ramp to 723 K (3 K /min) held for 2 h. The adsorption temperature of Pyridine (1 torr at equilibrium) and 2,6 Di-tert-butylpyridine (0.2 torr at equilibrium) were 373 K and 423 K, respectively. DMQ, TBA, THA, and TTBPy (0.1-0.2 torr) adsorptions were performed at 298 K. After equilibration with the probe molecules, the cell was outgassed to remove the physisorbed species. All spectra were normalized to the same mass (20 mg wafers). The amounts of pyridine adsorbed on the Brønsted and Lewis acid sites were determined by integrating the area of the characteristic bands corresponding to pyridinium ions (1545 cm^{-1}) and coordinated pyridine (1454 cm^{-1}) using their respective molar absorption coefficients (ε1545 =1.35 and ε1454 = 1.8 cm.mol^{-1}).([24]) As TTBPy is solid at room temperature (melting point: 343 K and boiling point: 393 K), an alternative procedure was followed for its adsorption. A self-supported wafer of solid TTBPy was first prepared and

transferred to a small calibrated volume enclosed between 2 valves in the IR cell (Figure S1). After evacuation under vacuum, this volume is isolated during the activation of the zeolite; the valve is then opened to start the TTBPy adsorption.

A homemade cell was used to perform the NMR experiments (Figure S.2). As outlined above, two different molecules were selected: *i*) Trimethylphosphine oxide (TMPO) to access both the internal and external acidity, *ii*) Triphenylphosphine oxide (TPhPO) to access only the external acidity. The samples were first dehydrated under vacuum (10^{-6} Torr) at 723 K (reached at 3 K /min) for 2 h, a solution of TMPO (4 mmol/l) or TPhPO (0.4 mmol/l) in CH_2Cl_2 then poured on the zeolite in a glove box filled with argon and equilibrated for 15 min under ultra-sonication. The cell was then connected to a vacuum line (Pressure = 10^{-4} torr) and evacuated at 298 K for 2 hours, the product recovered transferred to an argon filled glove box and loaded in an NMR rotor. The NMR spectra were recorded on a Bruker Avance 500 and the samples spun at the magic angle at a frequency of 12 kHz with a single pulse width of 8.5 µs and a recycle delay of 10 s. The ^{31}P chemical shifts were measured relative to an aqueous H_3PO_4 (85 %).

Table 1. Physico-chemical properties of the parent zeolite powders

Zeolite	**LZY-64**	**CBV720**	**CBV760**
Unit cell parameter (Å) [a]	24.7	24.3	24.2
$Si/Al_{Framework}$ [b]	2.3	16	28
V_{Micro} (cm^3/g) [c]	0.34	0.27	0.27
V_{Meso} (cm^3/g) [c]	0.05	0.23	0.27
S_{BET} (m^2/g) [c]	754	840	805
S_{Ext} (m^2/g) [c]	60	267	261
Crystallinity (%) [d]	100	70	70

[a] unit cell parameter; [b] determined by ^{29}Si MAS NMR; [c] determined by nitrogen sorption at 77K; [d] relative to LZY-64

RESULTS AND DISCUSSION

Adsorption of basic probe molecules monitored by IR

Internal and external acidity of the FAU structure: Pyridine (Py)

Figure1a shows the IR spectra of LZY-64 activated at 723 K before and after pyridine adsorption. After activation, three absorption bands are observed in the ν(OH) region:

- 3740 cm^{-1}: silanol groups

- 3640 cm^{-1} and 3545 cm^{-1}: bridging hydroxyl groups (Brønsted acid sites, BAS) respectively located in the supercages (OH_{HF}) and sodalite cages (OH_{LF}).

After pyridine adsorption and evacuation at 523 K, the supercages BAS (3640 cm^{-1}) disappear almost completely while those in the sodalite cages (3545 cm^{-1}) are unaffected, Figure 1. The number of BAS determined by this procedure is reported in Table 2. As expected, the majority of acidic sites accessible to pyridine are located in the supercages (1260 µmol/g) and the proportion of acidic sites accessible to pyridine in sodalite cages is negligible. The difference in the number of acid sites estimated by IR and ^{29}Si NMR for LZY-64 is a direct consequence of the presence of residual sodium cations (*ca.* 3 % determined by ICP analysis). The ACI of pyridine in LZY-64 is 0.4 and implies that only 40% of the acidic sites, all located in in the supercages, are accessible to molecules with a kinetic diameter of about 0.55 nm.

The same procedure is applied to CBV760, Figure 1b. In contrast to LZY-64, the acidic sites in the sodalite cages become accessible to pyridine as both OH_{HF} and OH_{LF} bands disappear after pyridine adsorption. While the number of Brønsted acid sites is much lower on CBV760, their accessibility to pyridine is higher (0.5), although the presence of extraframework aluminum could hinder access to some acid sites. The Brønsted acid site concentration expected from the ^{29}Si NMR derived framework composition (520 µmol/g) is significantly higher than those detected (320 µmol/g) and accessible (240 µmol/g) by IR spectroscopy.([65])

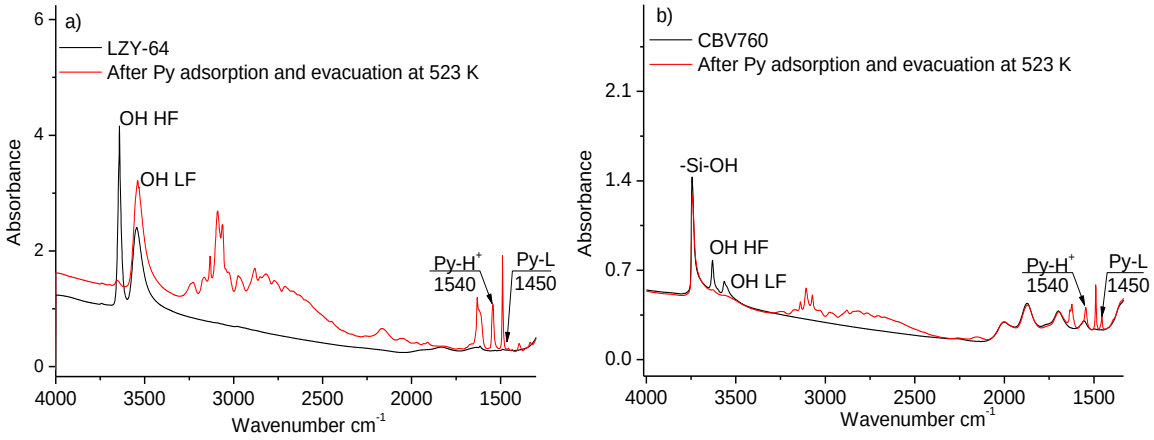

Figure 1. IR spectra before and after adsorption of pyridine and evacuation at 523 K under vacuum: *a)* LZY-64 and *b)* CBV760.

Table 2 : Acid site concentration in LZY-64 and CBV760.

Sample	OH_{HF} µmol/g [a]	OH_{LF} µmol/g [a]	Σ OH µmol/g [b]	Σ µmol/g [c]	Al^{IV}	$Py\text{-}H^+$ µmol/g [d]	Py-L [d] µmol/g	ACI_{Py} [e]
LZY-64	1260	2090	3350	3570		1390	45	0.4
CBV760	140	180	320	520		240	84	0.5

[a] determined using molar absorption coefficients of OH bands ([24])

[b] sum of all bridging hydroxyls: OH_{HF} + OH_{LF}

[c] tetrahedral (framework) aluminum calculated from the Si/Al ratios determined by ^{29}Si NMR

[d] $Py\text{-}H^+$: protonated pyridine (Brønsted sites), Py-L: coordinated pyridine (Lewis sites)

[e] accessibity index of pyridine = $Py\text{-}H^+/\Sigma\ Al^{IV}$

External acidity of the FAU structure: the case of 2,6 Di-tert-butylpyridine (DTBPy)

This bulky molecule (kinetic diameter: 0.8 nm) is already used to probe the external acidity of different zeolite types such as MOR, ZSM-5.([31,66]) However, on LZY-64 and CBV760, the OH_{HF} band (supercages) decreases upon DTBPy adsorption and evacuation at 523 K, while the OH_{LF} (sodalite cages) remains intact or slightly broadened, Figure 2. New bands appear at 3360, 1616 and 1530 cm^{-1}, characteristic of protonated DTBPy. The IR spectra of LZY-64 after exposure to DTBPy for 0-64 minutes are shown in Figure 3a and the variation of the integrated intensity of the 3360 cm^{-1} band (DTBPyH+) with the amount of OH_{HF} consumed (molar absorption of 6.76 µmol cm^{-1}) in Figure 3b. An excellent linear correlation (r^2 = 0.99) with a zero intercept allows to calculate the molar absorption coefficient ([5.22] $cm.\mu mol^{-1}$) of the 3360 cm^{-1} band of $DTBPyH^+$ assuming DTBPy adsorbs specifically on OHHF. The resulting number of acidic sites (1013 µmol/g) probed by 2,6 DTBPy is reported in Table 3.

While this demonstrates an expected lower accessibility of DTBPy than Py to both LZY-64 and CBV760 acid sites, DTBPy nevertheless interacts with internal acidity, including sodalite cages in CBV760. Therefore it cannot be considered a suitable probe for the external surface of FAU structures.

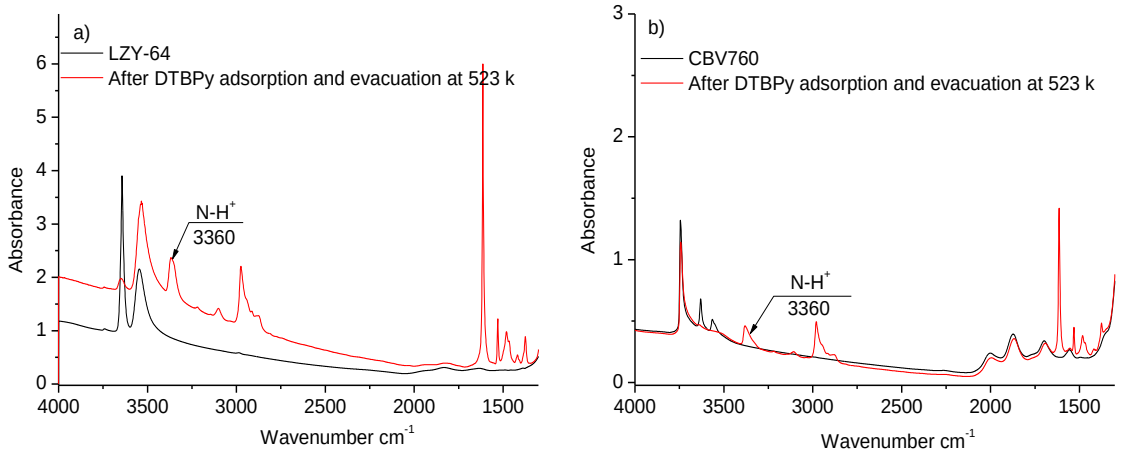

Figure 2. IR spectra before and after adsorption of 2,6 Di-tert-butylpyridine (DTBPy) and after evacuation at 523 K under vacuum: *a)* LZY-64 and *b)* CBV760.

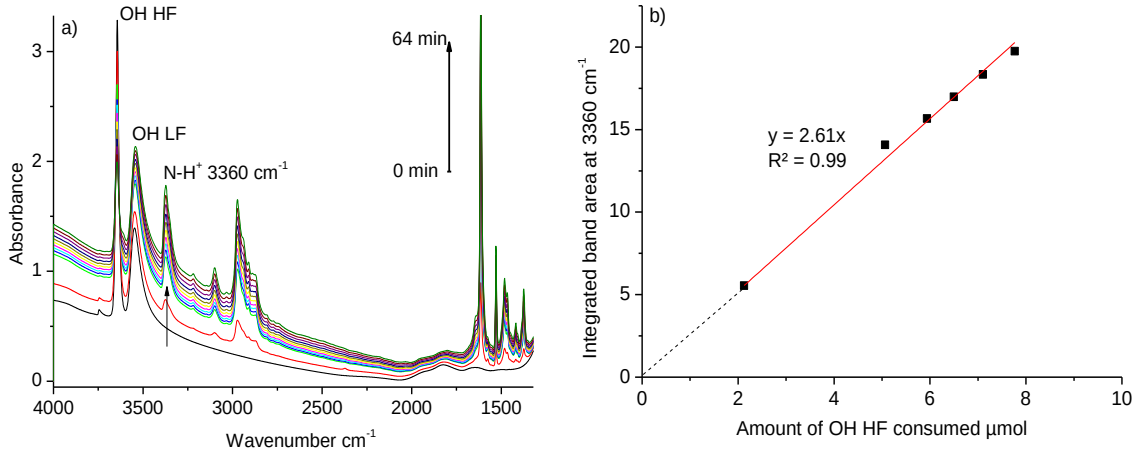

Figure 3. *a)* Time evolution of the IR spectra of LZY-64 in contact with 2,6 DTBPy, *b)* integrated band area at 3360 cm^{-1} as a function of the OH_{HF} consumed.

Table 3. Acidic properties of LZY-64 and CBV760 probed by Py and DTBPy.

Sample	Σ Al^{IV} µmol/g [a]	Py-H^+ µmol/g [b]	ACI_{Py} [c]	DTBPy-H^+ µmol/g [d]	ACI_{DTBP} [e]
LZY-64	3565	1391	0.4	1013	0.3
CBV760	520	240	0.5	197	0.4

[a] concentration of framework aluminum determined by ^{29}Si NMR

[b] Py-H^+: concentration of Pyridine adsorbed on Brønsted acid sites after evacuation at 423 K

[c] accessibity index of pyridine = Py-H^+/ Σ Al^{IV}

[d] DTBPy-H^+: concentration of DTBPy adsorbed on Brønsted acid sites after evacuation at 423 K

[e] accessibity index of 2,6 DTBPy = DTBPy-H^+/ Σ Al^{IV}

External acidity of the FAU structure: a quest for the right molecule

n-Tributylamine (TBA), 2,4 dimethylquinoline (DMQ), n-trihexylamine (THA) and 2,4,6 tri-tert-butylpyridine (TTBPy) are selected as their adsorption/diffusion in the microporosity at 298 K might become slow enough to discriminate between internal and external acidity during IR monitored uptake experiments. As discussed above, the amount of adsorbed probe molecules is determined by following the consumption of the OH bands (molar absorption coefficients from Ref. 24) assuming one probe molecule adsorbs per acid site. Figure 4 shows the disappearance of the OH_{HF} (3640 cm^{-1}) band of LZY-64 as a function of $\sqrt{t}$ (t = exposure time, in s) at 298 K for these candidates. Except for TTBPy and THA, a monotonous uptake of the probe molecule is observed.

DTBPy, often used to probe the external acid sites of large pore zeolites (MOR, BEA…) zeolites, enters the microporosity of LZY-64, and reaches about 16 % of the acid sites within 20 min. Both TBA and DMQ behave similarly, albeit slower. DMQ, for instance reaches 16 % of the acidic sites, after 1 hour at 298 K. THA on the other hand first adsorbs slowly, reaching a plateau after consuming about 2 % of the acid sites, to finally reach 14 % of the Bronsted sites after 2 hours. The plateau corresponds to the expected quantity of THA adsorbed on the external surface sites, in good agreement with earlier computed geometric external surface of zeolite Y.([67]) In the case of this particular LZY-64, its geometric surface evaluated assuming spherical crystallites (500 nm diameter) and no Al zoning, as described elsewhere, ([58,71]) amounts to 10 m^2/g, *i.e.* the external acid sites contribute to about 1.3 % of the total acidity, *i.e.* 45 µmol/g of zeolite.

In contrast to the above probes, liquid at room temperature, the TTBPy uptake is slow and progressive reaching a final plateau when about 2 % of the acid sites are neutralized (inset in Figure 4) indicating that it never accesses the microporosity at 298 K and interacts only with the external Brønsted acidity. Again, assuming that one molecule is adsorbed per acid site, the external acid sites of zeolite is estimated to 50 µmol/g. However, at a higher temperature, 373 K, TTBPy penetrates zeolite Y microporosity.

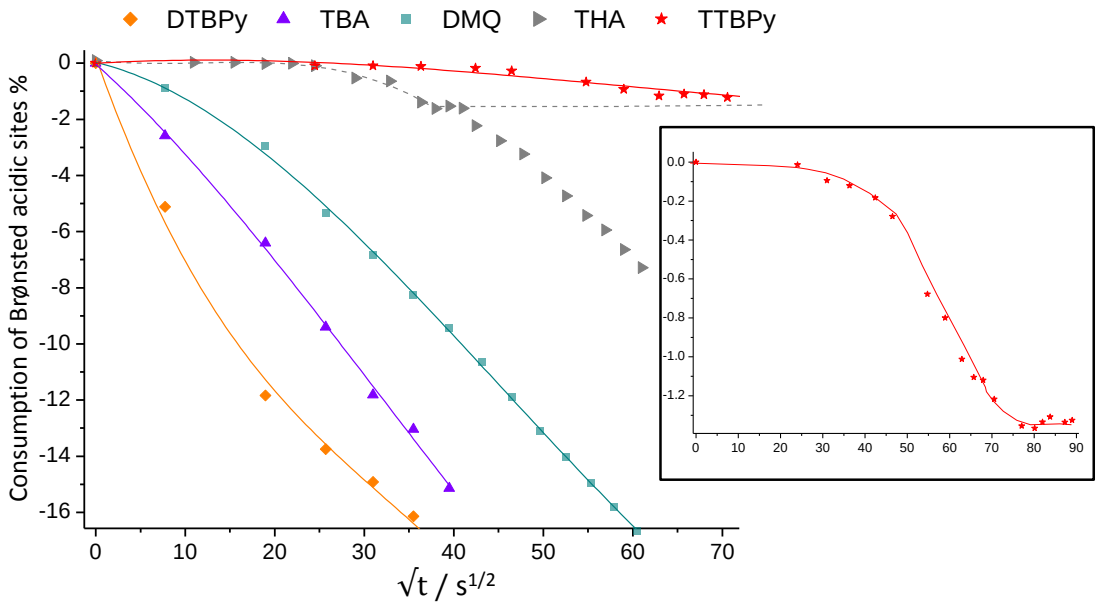

Figure 4. Consumption of the LZY-64 Brønsted acidity as a function of the square root of exposure time ,$\sqrt{t}$, at 298 K for various basic probe molecules (inset: zoom on TTBPy).

In order to better quantify the TTBPy adsorbed on the BAS of the USY zeolites, with higher Si/Al, the molar extinction coefficient of its protonated form, $TTBPy^+$, is determined, *vide infra*. Figure 5 shows the spectra of TTBPy vapor (a), 1 wt % TTBPy dispersed in KBr (b) and a difference spectrum *i.e.* the pristine LZY-64 spectra substracted form TTBPY adsorbed on LZY-64 (c). The latter displays new bands at 3365, 3350, 1612 and 1373 cm^{-1}. The 3365 and 3350 cm^{-1} are assigned to ν(N-H+) vibrations of protonated TTBPy.([68]) The molar absorption coefficient of the ν(N-H+) band at 3365 cm^{-1} is determined as for 2,6 DTBPy, vide supra.

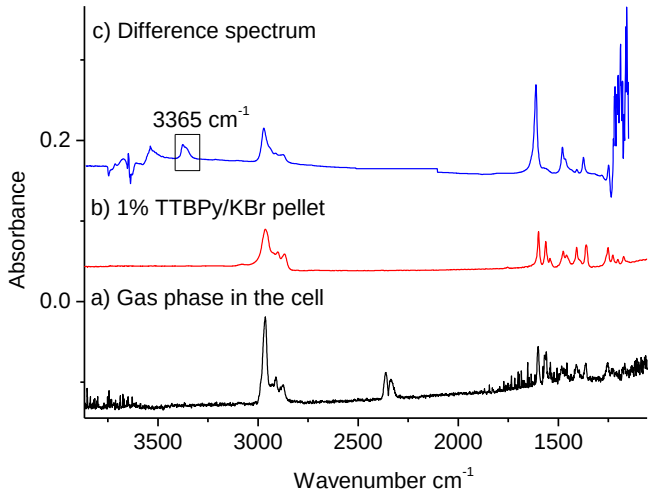

Figure 5. IR spectra of a) gas phase (TTBPy) in the cell (x 40), b) 1% TTBPy/KBr pellet, c) difference spectrum between TTBPY adsorbed on LZY-64 and the pristine LZY-64 (298 K).

The $TTBPyH^+$ (3370-3350 cm^{-1}) integrated area correlates (r^2 = 0.99) well with the intensity decrease of the OH_{HF}, (Figure 6 b). The derived molar absorption coefficient, ε, is 5.74 cm.µmol^{-1}. TTBPy is also adsorbed on CBV720 and CBV760 (298 K followed by evacuation under vacuum at RT for 15 min) and compared with LZY-64 (Figure 7). This confirms that on LZY-64, as with Py and DTBPy, only the OH_{HF} band decreases while the OH_{LF} broadens. Table 4 summarizes the TTBPy results on the three zeolites and the associated accessibilities (ACI).

On that basis, we conclude that THA and TTBPy are suitable molecules to probe the external surface of FAU; TTBPy should be preferred as it does not enter the zeolite microporosity, even after upon prolonged exposure.

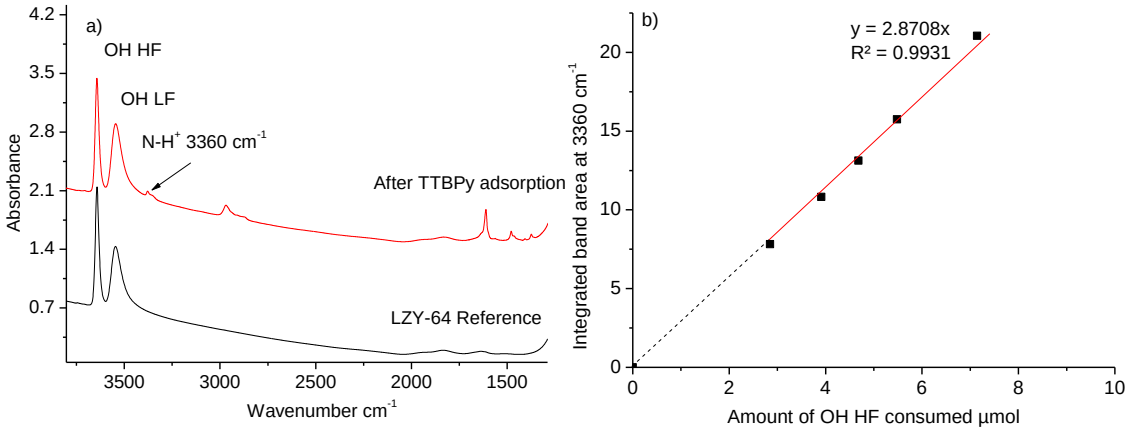

Figure 6. *a)* IR spectra of LZY-64 before and after 120 min contact with TTBPY vapor at 298 K, *b)* integrated intensity of the 3360 cm^{-1} band as a function of OH_{HF} consumed.

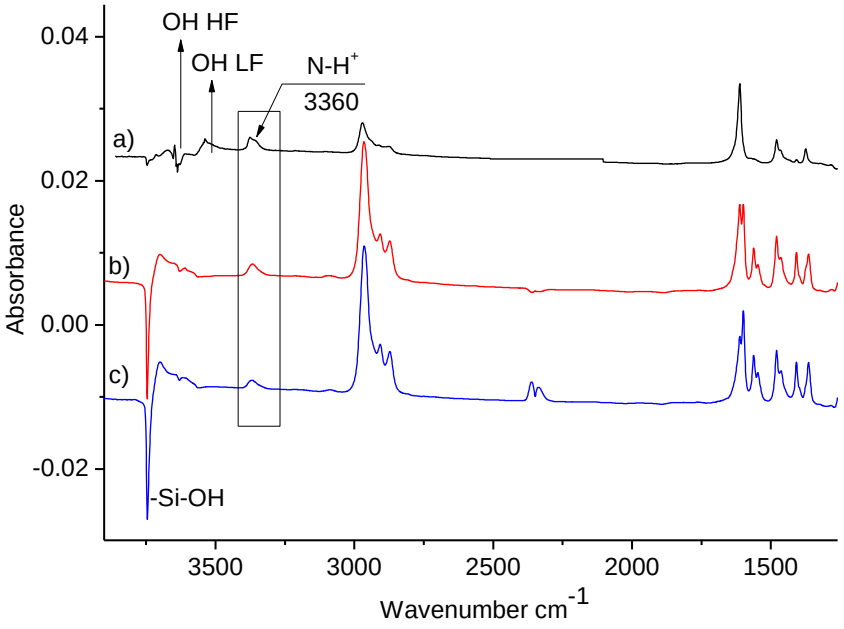

Figure 7. IR spectra of TTBPy adsorbed at 298 K and evacuated under vacuum at room temperature for 15 min on *a)* LZY-64, *b)* CBV720, *c)* CBV760.

Table 4. External acidity of LZY-64, CBV720 and CBV760 zeolites probed by TTBPy.

Zeolite	TTBPy-H^+ $_{\mu mol/g}$ [a]	ACI $_{TTBPY}$ [b]
LZY-64	60	0.02
CBV720	24	0.04
CBV760	20	0.04

[a] TTBPy-H^+: Tri-tert-butylpyridine molecules adsorbed on Brønsted sites after evacuation

[b] accessibility index of TTBPy = TTBPy-H^+ / Σ Al^{IV}

Adsorption of basic probe molecules monitored by ^{31}P NMR

Internal and external acidity of the FAU structure: Trimethylphosphine oxide (TMPO)

LZY-64 and CBV760 zeolites are loaded with an excess of TMPO to guarantee a complete titration of all acid sites (4 mmol of TMPO/g zeolite, dissolved in 1 ml of CH_2Cl_2). When all acid sites are titrated, a peak due to physisorbed (solid) TMPO emerges between 39-43 ppm and serves as an internal standard.

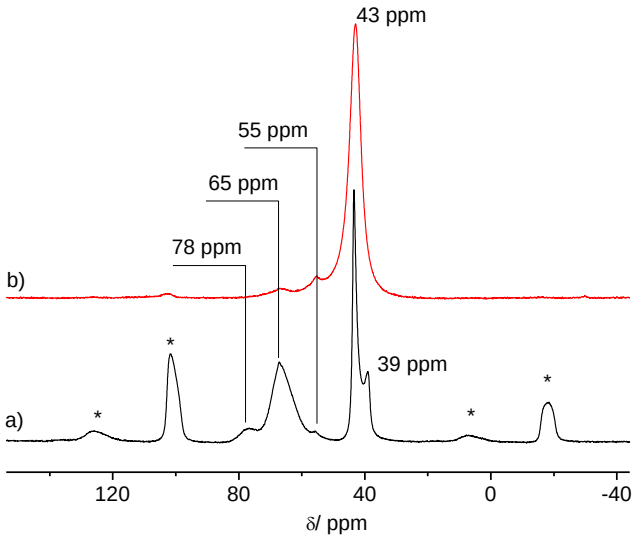

Figure 8. ^{31}P MAS NMR spectra of TMPO adsorbed on *a)* LZY-64, *b)* CBV760 (*: spinning side bands).

It is well established that TMPO accesses the microporosity of zeolite Y.([46]) The ^{31}P NMR MAS spectrum of pure TMPO, Figure S.3, displays two signals at 39 and 43 ppm. The first is assigned to crystalline TMPO while the second is due to interaction between P=O and traces of water.([69,33,69,70]) Figure 8 shows the ^{31}P NMR spectra of TMPO adsorbed on LZY-64 and CBV760. On LZY-64, three signals in the 55-80 ppm range are assigned to Brønsted acid sites.([45,48,49,50]) Obenaus *et al.* assigned the 55 ppm resonance to TMPO interacting with Brønsted acid sites in the sodalite cages, while those at 65 and 78 ppm to the Brønsted acid sites located in the supercages.([71]) The ^{31}P NMR spectrum of CBV760 shows similar features to LZY-64, except the 78 ppm resonance. The number of acid sites measured by TMPO in LZY-64 is therefore 3046 µmol/g showing that, as expected, TMPO interacts with almost all acid sites, including those located in sodalite cages (ACI = 0.85).

External acidity of the FAU structure: Triphenylphosphine oxide (TPhPO)

TPhPO is a bulky molecule (kinetic diameter of of 1.1 nm) previously used by Ryoo *et al.* to measure the external acidity of highly mesoporous MFI structures.([33,72]) As it should have a highly restricted access to the zeolite Y microporosity, it is a potential candidate to interact specifically with its external acidic sites. The ^{31}P NMR spectrum of pure TPhPO, displays two resonances, 24 ppm and 28 ppm, assigned respectively to crystalline TPhPO and hydrated TPhPO due, as for TMPO, to interactions between P=O and traces of water as, Figure 9. Upon adsorption on LZY-64 and CBV760, its ^{31}P NMR spectra display three resonances around 24, 28 and 30 ppm. On γ-alumina, the 28 ppm resonance of adsorbed TPhPO is attributed to its interaction with Lewis acid sites (Figure S.4). However, on a zeolite, TPhPO is too sterically hindered to interact with Lewis acidic sites. By analogy with TMPO, *vide* supra, we assign the 28 ppm resonance to physisorbed TPhPO and the 30 ppm one to TPhPO adsorbed on Brønsted acidic sites. The amount of Bronsted sites accessible to TPhPO on LZY-64 (53 µmol/g) and CBV760 (19 µmol/g) are consistent with those obtained by IR with TTBPy, a molecule of similar size (Table 5).

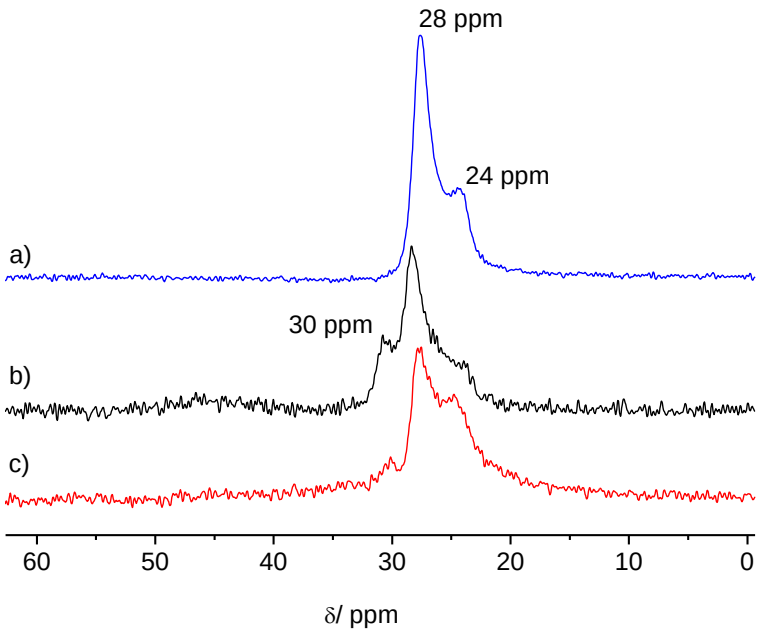

Figure 9. ^{31}P MAS NMR spectra of TPhPO *a)* pure, *b)* adsorbed on LZY-64, *c)* adsorbed on CBV760

Table 5. External acidity of LZY-64, CBV720 and CBV760 zeolites probed by TTBPy and TPhPO bulky basic molecules.

Zeolite	**Surface Brønsted acid site density µmol/g**	
	TTBPy (IR) [a]	**TPhPO (NMR)** [b]
LZY-64	60	53
CBV720	24	25
CBV760	20	19

[a] TTBPy: Tri-tert-butylpyridine molecules adsorbed on Brønsted sites

[b] TPhPO: Tri-phenylphosphine oxide molecules adsorbed on Brønsted sites

CONCLUSIONS

For the first time, the Brønsted acidity of the external surface of the FAU type structure, the archetype large pore zeolite, is measured. It is quantified by titration with probe molecules monitored by readily available and proven spectroscopic techniques, IR and NMR. Some bulky but flexible molecules (Tri-hexylamine, 1.3 x 1.4 nm) access both its external and internal acidity even when adsorption takes place at room temperature while others, less flexible (Tri-tert-butyl pyridine and Tri-phenylphosphine oxide, both 1.1 x 1.1) probe only the external acidity. The room temperature adsorption of tri-tert-butylpyridine monitored by IR spectroscopy indicates that 2 w% (Y) and 4 w% (USY) of the total acid sites, *i.e.* 60 µmol/g and 20 µmol/g respectively are located on the external surface. ^{31}P NMR spectroscopy of adsorbed triphenylphosphine oxide (TPhPO) leads to very similar conclusions.

This advance opens the door to a more quantitative and deeper understanding of the catalytic performances of zeolites, in particular, the nanosized and hierarchical ones where the external surface plays an even more important role.([43]) It will participate to a better description of structure-reactivity using the Thiele modulus approach and bring more insights in the structural and chemical changes occurring during the shaping of zeolites in technical bodies as this operation affects mainly the external surface, as reported recently.([16])

More insight is however required to establish better structure-activity correlations and design superior zeolitic catalysts. For instance, advanced NMR techniques ([69]) should bring more knowledge on the exact nature of the external acid sites while recent methodologies where calorimetric data are acquired together with the IR spectra of adsorbed probe molecules could provide information on the strength and the environment (confinement) of these acid

sites.([73]) Last but not least, advances in computational modelling will become ever more helpful to better understand the role of the external surface of zeolites, the compulsory ports of entry to their micropores.([19])

ASSOCIATED CONTENTS

Supporting Information is available free of charge via the Internet at http://pubs.acs.org : Physical properties and molecular dimensions of the basic probe molecules, schemes of the infrared and NMR cells and ^{31}P NMR spectra of the phosphorous based probe molecules.

AUTHOR INFORMATION

Corresponding Author
* Email: jean-pierre.gilson@ensicaen.fr.
* Email: suheil.abdo@honeywell.com.

Funding sources

Honeywell UOP

ACNOWLEDGMENT

Honeywell UOP for funding and permission to publish

SYNOPSIS TOC

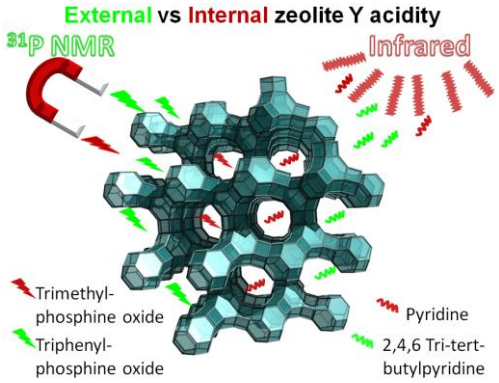

REFERENCES

(1) Rigutto, M. S.; Van. Veen, R.; Huve, L. Introduction to Zeolite Science and Practice, Vol. 168 ed. Čejka, J. ;Van Bekkum, H.; Corma, A.; Schüth, F. Elsevier, Amsterdam **2007**, 855-914.

(2) Kulprathipanja, S.; Zeolites in Industrial Separation and Catalysis, Wiley-VCH, Weinheim, Germany **2010**.

(3) Marcilly, C.; Acido-Basic Catalysis – Application to Refining and Petrochemistry, Editions Technip, Paris **2005**.

(4) Sheldon, R. A.; Van Bekkum, H. Fine Chemicals Through Heterogeneous Catalysis, Wiley-VCH, Weinheim **2000**.

(5) Ennaert, T.; Van Aelst, J.; Dijkmans, J.; De Clercq, R.; Schutyser, W.; Dusselier, M.; Verboekend, D.; Sels, B. F. Potential and challenges of zeolite chemistry in the catalytic conversion of biomass. *Chem. Soc. Rev.* **2016**, 45, 584-611.

(6) Vermeiren, W.; Gilson, J.-P. Impact of Zeolites on the Petroleum and Petrochemical Industry. *Top Catal.* **2009**, 52, 1131-1161.

(7) Van den Berg, J.; Gascon, J.; Kapteijn, F. in Zeolites and Catalysis – Synthesis, Reactions and Applications, ed. Cejka, J.; Corma, A.; Zones, S. I. Wiley-VCH, Weinheim **2010**, 361-387.

(8) Chen, N. Y.; Degnan, T. F.; Morris, C. Molecular Transport and Reaction in Zeolites, Wiley-VCH, Weinheim **1994**.

(9) Schwieger, W.; Gonche Machoke, A.; Reiprich, B.; Weissenberger, T.; Selvam, T.; Hartmann, M. Zeolites in Catalysis: Properties and Applications Čejka, J.; Morris R. E. eds. the Royal Society of Chemistry **2017**, 103-145.

(10) Cohen, D.; Merchuk, J.; Zeiri, Y.; Sadot, O. Catalytic effectiveness of porous particles: A continuum analytic model including internal and external surfaces. *Chem. Eng. Sci.* **2017**, 166, 101-106.

(11) Thommes, M.; Kaneko, K.; Neimark, A. V.; Olivier, J. P.; Rodriguez-Reinoso, F.; Rouquerol, J.; Sing, K. S. W.; Physisorption of gases with special reference to the evaluation of surface area and pore size distribution. *Pure Appl. Chem.* **2015**, 87, 1051-1069.

(12) Von Ballmoos, R.; Meier W. M. Zoned aluminium distribution in synthetic zeolite ZSM-5. *Nature* **1981**, 289, 782-783.

(13) Derouane, E. G.; Gilson, J.-P.; Gabelica, Z.; Mousty-Desbuquoit, C.; Verbist, J. Concerning the aluminum distribution gradient in ZSM-5 zeolites. *J. Catal.* **1981**, 71, 447-448.

(14) Van Bokhoven, J.; Danilina, D. Aluminum in Zeolites: Where is it and what is its structure? in Zeolites and Catalysis, Čejka, J.; Corma, A.; Zones, S. eds. Wiley-VCH, Weinheim **2010**, 283-298.

(15) Kraushaar-Czarnetzki, B. Shaping of Solid Catalysts, in Synthesis of Solid Catalysts, De Jong, K. P. ed. Wiley-VCH, Weinheim **2009**, 173-199.

(16) Lakiss, L.; Gilson, J. -P.; Valtchev, V.; Mintova, S.; Vicente, A.; Vimont, A.; Bedard, R.; Abdo, S.; Bricker, J. Shaping Zeolite Y Catalysts by Extrusion: Characterization and Catalytic Consequences of Zeolite-Binder Interactions. submitted to Microporous Mesoporous Mater.

(17) Derouane, E. G. Shape selectivity in catalysis by zeolites: The nest effect . *J. Catal.* **1986**, 100, 541-544.

(18) Wang, S.; Iglesia, E. Catalytic diversity conferred by confinement of protons within porous aluminosilicates in Prins condensation reactions. *J. Catal.* **2017**, 352, 415-435.

(19) Rey, J.; Raybaud, P.; Chizallet, C. Ab Initio simulation of the acid sites at the external surface of zeolite Beta. *ChemCatChem* **2017**, 9, 2176-2185.

(20) Gorte, R. J. What do we know about the acidity of solid acids? *Catal. Lett*. **1999**, 62, 1-13.

(21) Corma, A.; Fornes, V.; Melo, F. V.; Herrero, J. Comparison of the information given by ammonia t.p.d. and pyridine adsorption-desorption on the acidity of dealuminated HY and LaHY zeolite cracking catalysts. *Zeolites* **1987**, 7, 559-563.

(22) Tonetto, G.; Atias, J.; De Lasa, H. FCC catalysts with different zeolite crystallite sizes: acidity, structural properties and reactivity. *Appl. Catal.* A **2004**, 270, 9-25.

(23) Oliviero, L.; Vimont, A.; Lavalley, J. C.; Romero Sarria, F.; Gaillard, M.; Maugé, F. 2,6-Dimethylpyridine as a probe of the strength of Brønsted acid sites: study on zeolites. Application to alumina. *Phys. Chem. Chem. Phys*. **2005**, 7, 1861-1869.

(24) Thibault-Starzyk, F.; Gil, B.; Aiello, S.; Chevreau, T.; Gilson, J.-P. In situ thermogravimetry in an infrared spectrometer: an answer to quantitative spectroscopy of adsorbed species on heterogeneous catalysts. *Microporous Mesoporous Mater*. **2004**, 67, 107-112.

(25) Zecchina, A.; Spoto, G.; Bordiga, S. Probing the acid sites in confined spaces of microporous materials by vibrational spectroscopy. *Phys. Chem. Chem. Phys.* **2005**, 7, 1627-1642.

(26) Bordiga, S.; Lamberti, C.; Bonino, F.; Travert, A.; Thibault-Starzyk, F. Probing zeolites by vibrational spectroscopies. *Chem. Soc. Rev*. **2015**, 44, 7262-7341.

(27) Gilson, J.-P.; Fernandez, C.; Thibault-Starzyk, F. New insights on zeolite chemistry by advanced IR and NMR characterization tools. *J. Mol. Catal. A: Chemical* **2009**, 305, 54-59.

(28) Lercher, J. A.; Grundling, C.; Eder-Mirth, G. Infrared studies of the surface acidity of oxides and zeolites using adsorbed probe molecules. *Catal. Today* **1966**, 353-376.

(29) Vimont, A.; Thibault-Starzyk, F.; Daturi, M. Analysing and understanding the active site by IR spectroscopy. *Chem. Soc. Rev.* **2010**, 39, 4928-4950.

(30) Sarria, F. R.; Blasin-Aube, V.; Saussey, J.; Marie, O.; Daturi, M. Trimethylamine as a Probe Molecule To Differentiate Acid Sites in Y−FAU Zeolite: FTIR Study. *J. Phys. Chem. B* **2006**, 110, 13130-13137.

(31) Corma, A.; Fornes, V.; Forni, L.; Marquez, F.; Martinez-Triguero, J.; Moscottiy, D. 2, 6-Di-tert-butyl-pyridine as a probe molecule to measure external acidity of zeolites. *J. Catal.* **1998**, 179, 451-458.

(32) Hunger, M. Brønsted Acid Sites in Zeolites Characterized by Multinuclear Solid-State NMR Spectroscopy. *Catal. Rev. Sci. Eng*. **1997**, 39, 345-393.

(33) Zheng, A.; Liu, S. B.; Deng, F. ^{31}P NMR Chemical Shifts of Phosphorus Probes as Reliable and Practical Acidity Scales for Solid and Liquid Catalysts. *Chem. Rev.* **2017**, 117, 12475-12531.

(34) Choudhary, V. R.; Akolekar, D. B. Comparison of the acidity/site energy distribution in catalytically important zeolites. *J. Catal.* **1989**, 119, 525-530.

(35) Thibault-Starzyk, F.; Abelló, S.; Bonilla, A.; Thomas, K.; Fernandez, C.; Gilson, J.-P.; Ramírez, J. P. Quantification of enhanced acid site accessibility in hierarchical zeolites–the accessibility index. *J. Catal.* **2009**, 264, 11-14.

(36) Maache, M.; Janin, A.; Lavalley, J. C.; Benazzi, E. FT infrared study of Brønsted acidity of H-mordenites: Heterogeneity and effect of dealumination. *Zeolites* **1995**, 15, 507-516.

(37) Nesterenko, N. S.; Thibault-Starzyk, F.; Montouilliout, V.; Yushchenko, V. V.; Fernandez, C.; Gilson, J.-P.; Fajula, F.; Ivanova, I. I. The use of the consecutive adsorption of pyridine bases and carbon monoxide in the IR spectroscopic study of the accessibility of acid sites in microporous/mesoporous materials. *Kinetics and Catal*. **2006**, 7(1), 40-48.

(38) Freitas, C.; Barrow, N. S.; Zholobenko, V. Accessibility and Location of Acid Sites in Zeolites as Probed by Fourier Transform Infrared Spectroscopy and Magic Angle Spinning Nuclear Magnetic Resonance. *Johnson Matthey Technol.* Rev. **2018**, 62(3), 279-290.

(39) Armaroli, T.; Bevilacqua, M.; Trombetta, M.; Milella, F.; Alejandre, A. G.; Ramirez, J.; Notari, B.; Willey, R. J.; Busca, G. A study of the external and internal sites of MFI-type zeolitic materials through the FT-IR investigation of the adsorption of nitriles. *Appl. Catal. A: Gen.* **2001**, 216 (1-2), 59-71.

(40) Bevilacqua, M.; Meloni, D.; Sini, F.; Monaci, R.; Montanari, T.; Busca, G. A study of the nature, strength, and accessibility of acid sites of H-MCM-22 zeolite. *J. Phys. Chem. C* **2008**, 112, 9023-9033.

(41) Bevilacqua, M.; Busca, G. A study of the localization and accessibilty of Brønsted and Lewis acid sites of H-Mordenite through the FT-IR spectroscopy of adsorbed branched nitriles. *Catal. Commun.* **2002**, 3, (11), 497-502.

(42) Montanari, T.; Bevilacqua, M.; Busca, G. Use of nitriles as probe molecules for the accessibility of the active sites and the detection of complex interactions in zeolites through IR spectroscopy. *Appl. Catal. A: Gen.* **2006**, 307, (1), 21-29.

(43) Tzoulaki, D.; Jentys, A.; Pérez-Ramírez, J.; Egeblad, K.; Lercher, J. A. On the location, strength and accessibility of Brønsted acid sites in hierarchical ZSM-5 particles. *Catal. Today* **2012**, 198, 1,3-11.

(44) Gallas, J.-P.; Goupil, J. M.; Vimont, A.; Lavalley, J. C.; Gil, B.; Gilson, J. -P.; Miserque, O. Quantification of Water and Silanol Species on Various Silicas by Coupling IR Spectroscopy and in-Situ Thermogravimetry. *Langmuir* **2009**, 25, 5825-5834**.**

(45) Yu, S.; Tian, H. Acidity characterization of rare-earth-exchanged Y zeolite using ^{31}P MAS NMR. *Chinese Journal of Catal.* **2014**, 35, 1318-1328.

(46) Sutovich, K. J.; Peters, A. W.; Rakiewicz, E. F.; Wormsbecher, R. F.; Mattingly, S. M.; Mueller, K. T. Simultaneous Quantification of Brønsted and Lewis-Acid Sites in a USY Zeolite. *J. Catal.* **1999**, 183, 155-158.

(47) Guan, J.; Li, X.; Yang, G.; Zhang, W.; Liu, X.; Han, X.; Bao, X. Interactions of phosphorous molecules with the acid sites of H-Beta zeolite: Insights from solid-state NMR techniques and theoretical calculations. *J. Mol. Catal. A: Chemical* **2009**, 310, 113-120.

(48) Rakiewicz, E. F.; Peters, A. W.; Wormsbecher, R. F. Characterization of Acid Sites in Zeolitic and Other Inorganic Systems Using Solid-State ^{31}P NMR of the Probe Molecule Trimethylphosphine Oxide. J. Phys. Chem. B **1998**, 102, 2890-2896.

(49) Karra, M. D.; Sutovich, K. J.; Mueller K. T. NMR Characterization of Bronsted Acid Sites in Faujasitic Zeolites with Use of Perdeuterated Trimethylphosphine Oxide. *J. Am. Chem. Soc.* **2002**, 124(6), 902-903.

(50) Wiper, P. V.; Amelse, J.; Mafra, L. Multinuclear solid-state NMR characterization of the Brønsted/Lewis acid properties in the BP HAMS-1B (H-[B]-ZSM-5) borosilicate molecular sieve using adsorbed TMPO and TBPO probe molecules. *J. Catal.* **2014**, 316, 240–250.

(51) Baltusis, L.; Frye, J. S.; Maciel, G. E. Phosphine oxides as NMR probes for adsorption sites on surfaces. *J. Am. Chem. Soc.* **1986**, 108, 7119-7120.

(52) Sang, H.; Chu, H. Y.; Lunsford, J. H. An NMR study of acid sites on chlorided alumina catalysts using trimethylphosphine as a probe. *Catal. Lett.* **1994**, 26, 235-246.

(53) Lunsford, J. H.; Rothwell, W. P.; Shen, W. Acid sites in zeolite Y: a solid-state NMR and infrared study using trimethylphosphine as a probe molecule. *J. Am. Chem. Soc.* **1985**, 107, 1540-1547.

(54) Gilson, J.-P.; Derouane, E. G. On the external and intracrystalline surface catalytic activity of pentasil zeolites. *J. Catal.* **1984**, 88, 538-541.

(55) Kunkeler, P. J.; Downing, R. S.; Van Bekkum, H. The use of Bulky Molecules as Probes for Investigating the Contributions of the External and Internal Pore-wall Activities of Zeolite Catalysts. *Stud. Surf. Sci. Catal.* **2001**, 137, 987-1002.

(56) Weitkamp, J.; Ernst, S.; Puppe L. Shape-Selective Catalysis in Zeolites. Weitkamp J.; Puppe L. (eds.), Catalysis and Zeolites, Springer-Verlag Berlin Heidelberg **1999**, 327-376.

(57) Degnan, T. F. The implications of the fundamentals of shape selectivity for the development of catalysts for the petroleum and petrochemical industries. *J. Catal.* **2003**, 216, 32-46.

(58) Chen, C. S. H.; Schramm, S. E. Type and catalytic activity of surface acid sites of medium and large pore zeolites Their deactivation with bulky organophosphorus compounds. *Microporous Materials* **1996**, 7, 125-132.

(59) Chen, N. Y. Personal Perspective of the Development of Para Selective ZSM-5 Catalysts. *Ind. Eng. Chem. Res.* **2001**, 40, 4157-4161.

(60) Kaduk, J. A.; Faber, J. Crystal structure of zeolite Y as a function of ion exchange. *J. Rigaku* **1995**, 12(2), 14-34.

(61) Qin, Z.; Cychosz, K. A.; Melinte, G.; El Siblani, H.; Gilson, J.-P.; Thommes, M.; Fernandez, C.; Mintova, S.; Ersen, O.; Valtchev, V. Opening the Cages of Faujasite-Type Zeolite. *J. Am. Chem. Soc.* **2017**, 139, 17273-17276.

(62) Mintova, S.; Gilson, J.-P.; Valtchev, V. Advances in nanosized zeolites. *Nanoscale* **2013**, 5, 6693-6703.

(63) Awala, H.; Gilson, J.-P.; Retoux, R.; Boullay, P.; Goupil, J. M.; Valtchev, V.; Mintova, S. Template-free nanosized Faujasite-type zeolites. *Nature Mat.* **2015**, 14, 447-451.

(64) Van Koningsveld, H.; Jansen, J. C. Single crystal structure analysis of zeolite H-ZSM-5 loaded with naphthalene. *Microporous Mater.* **1996**, 6, 159-167.

(65) Almutairi, S. M. T.; Mezari, B.; Filonenko, G. A.; Magusin, P. C. M. M.; Rigutto, M. S.; Pidko, E. A.; Hensen, E. J. M. Influence of Extraframework Aluminum on the Brønsted Acidity and Catalytic Reactivity of Faujasite Zeolite. *ChemCatChem **2013***, 5, 452 - 466.

(66) Gora-Marek, K.; Tarach, K.; Choi, M. 2,6-Di-*tert*-butylpyridine Sorption Approach to Quantify the External Acidity in Hierarchical Zeolites. *J. Phys Chem C* **2014**, 118, 12266-12274.

(67) Farcasiu, M.; Degnan, T. The role of external surface activity in the effectiveness of zeolites. *Ind. Eng. Chem. Res.* **1988**, 27, 45-47.

(68) Lin-Vien, D.; Colthup, N. B.; Fateley, W. G.; Grasselli, J. G. The handbook of Infrared and Raman characteristic frequencies of organic molecules. Academic press **1991**, 163-168.

(69) Zheng, A. M.; Zhang, H. L.; Lu, X.; Liu, B. S.; Deng, F. 31P Chemical Shift of Adsorbed Trialkylphosphine Oxides for Acidity Characterization of Solid Acids Catalysts. *J. Phys. Chem. B* **2008**, 112, 4496-4505.

(70) Begimova, G.; Tupikina, E. Y.; Yu, V. K.; Denisov, G. S.; Bodensteiner, M.; Shenderovich, I. G. Effect of Hydrogen Bonding to Water on the 31P Chemical Shift Tensor of Phenyl- and Trialkylphosphine Oxides and α-Amino Phosphonates. *J. Phys. Chem. C* **2016**, 120, 8717-8729.

(71) Obenaus, U.; Dyballa, M.; Lang, S.; Scheibe, M.; Hunger, M. Generation and Properties of Brønsted Acid Sites in Bifunctional Rh-, Ir-, Pd-, and Pt-Containing Zeolites Y Investigated by Solid-State NMR Spectroscopy. *J. Phys. Chem. C* **2015**, 119, 15254-15262.

(72) Kyungsu, N.; Changbum, J.; Jeongnam, K.; Kanghee, C.; Jinhwan, J.; Yongbeom, S.; Messinger, J. R.; Chmelka, F. B.; Ryong, R. Directing Zeolite Structures into Hierarchically Nanoporous Architectures. *Science* **2011**, 333, 328-332.

(73) Stošić, D.; Bennici, S.; Sirotin, S.; Stelmachowski, P.; Couturier, J. L.; Dubois, J. L.; Travert, A.; Auroux, A. Examination of acid–base properties of solid catalysts for gas phase dehydration of glycerol: FTIR and adsorption microcalorimetry studies. *Catal. Today* **2014**, 226, 167-175.